SEA-SURFACE NRCS OBSERVATIONS IN HIGH WINDS AT LOW INCIDENCE ANGLES

Joseph Sapp, Paul Chang, Zorana Jelenak†*

NOAA/NESDIS/STAR/SOCD
College Park, MD, USA 20740

Stephen Frasier, Tom Hartley

University of Massachusetts Amherst
Microwave Remote Sensing Laboratory
Amherst, MA, USA 01003

ABSTRACT

We report on airborne measurements of the sea-surface normalized radar cross-section (NRCS) at incidence angles of approximately 22° obtained at both C-band and Ku-band in high-wind ($> 25\,\mathrm{m\,s^{-1}}$) conditions. Measurements obtained over numerous research flights through tropical cyclones and high-latitude winter storms between 2011 and 2014 are composited to yield geophysical model functions in rain-free conditions. The present observations extend the results of [1], who reported high-wind NRCS for incidence angles from 30° to 50°, to a smaller incidence angle. Saturation of the mean NRCS is observed at both frequencies. In some cases the NRCS is observed to decrease with increasing wind speed beyond the saturation. The results have implications for planned and future scatterometers aiming to increase the observed swath width by extending the range of incidence angles.

Index Terms— Radar remote sensing, airborne radar, radar cross-sections, sea measurements, C-band

1. INTRODUCTION

Since 2003, the Microwave Remote Sensing Laboratory (MIRSL) at the University of Massachusetts Amherst (UMass) has regularly operated an airborne scatterometer, the Imaging Wind and Rain Airborne Profiler (IWRAP), that utilizes both C- and Ku-band frequencies [2]. MIRSL has a data archive from this instrument dating back to 2005.

Ocean vector wind retrievals are based on the normalized radar cross-section (NRCS), or σ^0, measured from the ocean surface. NRCS is typically modeled by the function

$$\begin{aligned}\sigma^0\left(U_{10N},\theta,\chi,p,\lambda\right) =& A_0\left(U_{10N},\theta,p,\lambda\right)\cdot\left[\,1\right.\\ &+ a_1\left(U_{10N},\theta,p,\lambda\right)\cos\chi\\ &\left.+ a_2\left(U_{10N},\theta,p,\lambda\right)\cos 2\chi\,\right],\end{aligned}\tag{1}$$

where χ is the wind-relative azimuth angle, θ is the incidence angle, p is the polarization, and λ is the wavelength. The geophysical model function can be used to retrieve the most likely wind speed and direction that would produce the NRCS observed.

A_0 is the mean NRCS and has a strong response to wind speed. The parameterization of A_0 from (1) is chosen following the formulation in [1]:

$$\begin{aligned}A_0\left(U_{10N},\theta,p\right) =& 10^{\beta(U_{10N},\theta,p)}\cdot\left[U_{10N}\right]^{\gamma_0(U_{10N},\theta,p)}\\ &\cdot\left[U_{10N}\right]^{\gamma_1(U_{10N},\theta,p)\cdot\log(U_{10N})}\\ &\cdot\left[U_{10N}\right]^{\gamma_2(U_{10N},\theta,p)\cdot\log^2(U_{10N})},\end{aligned}\tag{2}$$

where U_{10N} is the 10 m equivalent neutral wind speed, θ is the incidence angle, and p is the polarization. The dependence of all these parameters on frequency band is implied.

2. INSTRUMENTATION

IWRAP, initially described in [2], is a dual-frequency conically-scanning Doppler radar developed by MIRSL that is routinely installed on the National Oceanic and Atmospheric Administration (NOAA) WP-3D research aircraft. IWRAP is primarily designed as a scatterometer, to study the signature of the ocean surface under wind forcing. Two pulsed radars, one C-band and one Ku-band, scan at two incidence angles each, typically between 20° and 50°. Each radar is capable of implementing up to four simultaneous beams, however, two simultaneous beams per radar has been the normal mode of operation since 2006. For the present study, incidence angles near 22° and co-polarized NRCS were used. The radar azimuthal beamwidths vary depending

*J. Sapp was with the University of Massachusetts Amherst; he is now with Global Science & Technology, Inc.

†UCAR

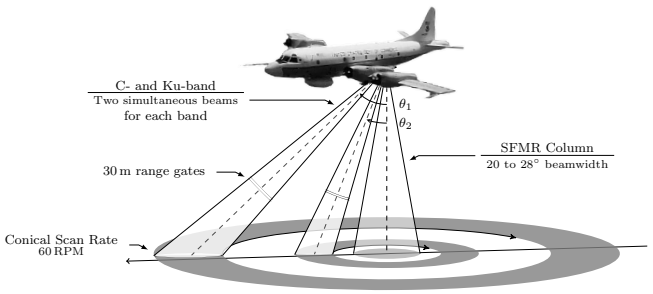

Fig. 1. Typical configuration of the IWRAP scatterometer/profiler instrument on the NOAA WP-3D aircraft. The incidence angle, conical scan rate, transmit and receive polarizations, pulse compression mode, pulse length, and pulse repetition frequency, among others, are all configurable.

upon the selected incidence angle, owing to properties of the frequency-scanned antenna, but are typically in the neighborhood of 10°. The antennas are mechanically scanned in azimuth, nominally at a rate of 1 Hz. A diagram of the typical configuration of IWRAP on the aircraft is shown in fig. 1.

The National Oceanic and Atmospheric Administration's Aircraft Operations Center (AOC) operates Stepped Frequency Microwave Radiometer (SFMR), developed by ProSensing, Inc. of Amherst, MA, that is used to retrieve surface wind speed and volume-averaged rain rate below the aircraft. It is a C-band nadir-pointing microwave radiometer that steps through six frequencies, dwelling at each for 0.5 s to make a brightness temperature (T_b) measurement. This instrument has been installed on each of the NOAA WP-3D aircraft for all research flights since 2006. Though the GMF relating excess emissivity from the ocean surface to surface wind speed was recently revised [3], the operational GMF from [4] is used in this analysis. Since the retrieval algorithm for SFMR is only reliable at nadir incidence, retrievals are only used from data collected at aircraft-nadir incidence angles within ±3°.

3. METHODOLOGY

To develop a new rain-free geophysical model function, IWRAP measurements and SFMR surface wind speed retrievals from selected flights between 2011 and 2014 are collocated. During these seasons, the frequencies used to generate the particular incidence angles on the IWRAP instrument were kept consistent—approximately 22° and 48° for both C- and Ku-band radars. The flights selected represent a variety of rain-free ocean conditions, including those of high-latitude winter storms and Category 3 hurricanes.

NRCS measurements from IWRAP are averaged into alongtrack cells of 2.5 km length. Each cell is divided into 64 track-relative azimuth bins, resulting in an average over 5.625° per bin. All radar beams for each polarization resulting in a surface echo within an alongtrack cell are averaged within these azimuth bins. SFMR and some location data are associated with an alongtrack cell only when the aircraft is over the cell. IWRAP data is only used when the aircraft is level (i.e., the instantaneous incidence angle of the radar beam is within ±2° of nominal) in order to limit the effects of non-uniform incidence angle. The surface wind direction is derived from the NRCS and, to avoid spurious direction estimates, the median over 5 cells (12.5 km) of continuous flight time is used as the true surface upwind direction for each cell. An additional protection is taken against erroneous direction estimates in high winds by using a surface wind vector model (GDAS or a direction estimate from the NOAA/NHC Atlantic HURDAT2). If the model wind direction for a cell is more than 90° away from the NRCS-estimated direction, the estimated direction is adjusted by 180°.

Any NRCS values affected by rain (as determined by IWRAP) are discarded. Additionally, any wind vector cell with an SFMR wind speed below $15\,\mathrm{m\,s^{-1}}$ or rain rate above $5\,\mathrm{mm\,h^{-1}}$ is discarded; these are the minimum values reliably retrievable from the SFMR [7].

The wind vector cells are grouped by SFMR wind speed in $2.5\,\mathrm{m\,s^{-1}}$ bins beginning at $15\,\mathrm{m\,s^{-1}}$. $2.5\,\mathrm{m\,s^{-1}}$ was chosen to account for the uncertainty of the SFMR retrievals. The data are shifted so upwind is at 0° azimuth and are averaged within azimuth bins, resulting in 64 points per wind speed bin.

These points are fit to the model described by (1). For each frequency, polarization, and incidence angle, one term from (1) is selected for fitting. This term is estimated for each $2.5\,\mathrm{m\,s^{-1}}$-wide bin via a least squares fit of the model for the term. Parameters of the selected term are derived using separate least squares fits to these estimates, with the independent vector chosen to be the center wind speeds of each bin. Except for γ_2, which is predetermined, all parameters are allowed to vary as required to minimize the χ^2 error.

4. RESULTS

Figure 2 shows the C-band A_0 estimates from the previous plots, GMFs, and the least-squares fits to the estimates. The plots are labeled with a vertical offset that is applied to both the IWRAP GMF and the data. A_0 estimates within $25\,\mathrm{m\,s^{-1}}$ to $27.5\,\mathrm{m\,s^{-1}}$ from each season are aligned vertically to match an existing IWRAP GMF in an attempt to remove calibration errors. The closest IWRAP GMFs to the data are near 30°. While this pro-

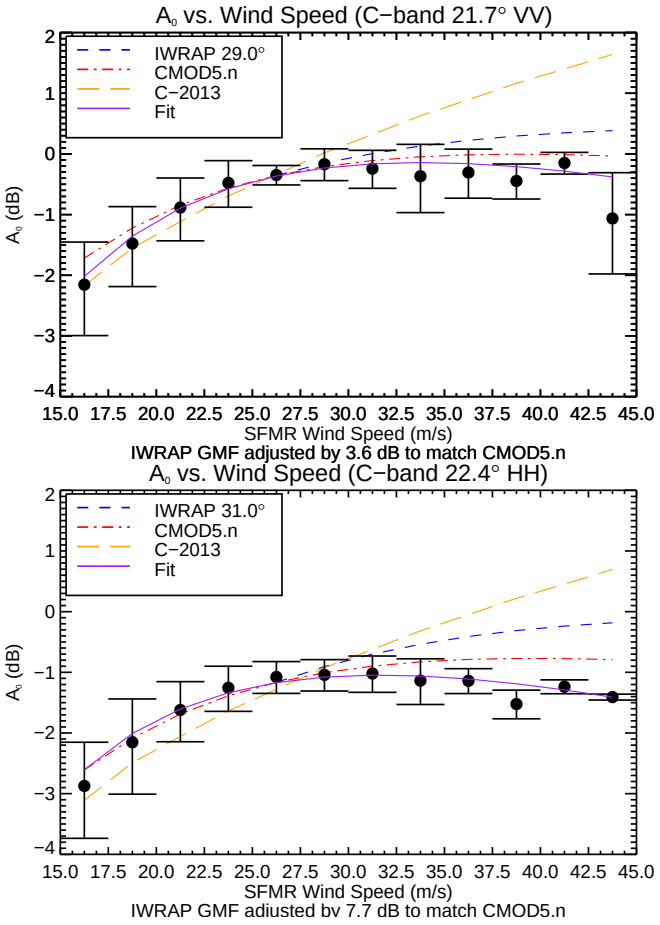

Fig. 2. C-band mean NRCS vs. wind speed (A_0 term) for 22° incidence, VV-polarization (top) and HH-polarization (bottom). A_0 data are shown as filled circles with the standard deviation of A_0 estimates from all wind vector cells shown as the error bars. C-band GMFs shown where valid are IWRAP (dashed), CMOD5.n (dash-dotted), and C-2013 (long dashes). The fit to the data is shown as a solid line.

cedure makes the calibration offset of each flight experiment the same, it does not necessarily remove the offsets. Here it is assumed that the CMOD5.n GMF more closely approaches the true A_0 value at these incidence angles, so a final alignment of the data and IWRAP GMF is performed to CMOD5.n at $25\,\mathrm{m\,s^{-1}}$. At HH-polarization, the alignment includes the polarization ratio from [6].

Because of the significant difference in incidence angle between these observations and the nearest IWRAP GMF (30°), the new data are not expected to match it. CMOD5.n slightly overestimates the mean NRCS above $30\,\mathrm{m\,s^{-1}}$, but the GMF was not developed for incidence angles less than 25°. At HH-polarization, the models are not expected to match the data as well as at VV. However, the behavior of CMOD5.n is just as good at HH as it is at VV below $30\,\mathrm{m\,s^{-1}}$. Saturation in the NRCS is observed at both polarizations at approximately $30\,\mathrm{m\,s^{-1}}$.

Figure 3 shows the Ku-band A_0 estimates, Ku-band GMFs, and fits to the estimates. The NSCAT2 algorithm is shown as a dash-dotted line and is used as the final calibration offset, like CMOD5.n is used above.

Data at HH-polarization match the IWRAP GMF reasonably well above $25\,\mathrm{m\,s^{-1}}$, despite the significant incidence angle difference. There may be some saturation occurring at the highest wind speeds, but it is difficult to determine without more samples. At VV-polarization, the observed NRCS stop increasing above $35\,\mathrm{m\,s^{-1}}$. Because of the data point in the highest wind speed bin, the fit decreases more rapidly with wind speed than at HH-polarization. As with HH-polarization, this may indicate saturation occurs at this incidence angle between $30\,\mathrm{m\,s^{-1}}$ and $40\,\mathrm{m\,s^{-1}}$.

5. CONCLUSIONS

Both the C-band and Ku-band observations show some apparent saturation of the NRCS at higher wind speeds. Additionally, the slope of the observed A_0 is relatively low over all wind speeds sampled. Beyond the saturation wind speed, C-band HH-polarization shows a marked decrease in A_0 while VV-polarization shows a slight decrease.

The saturation effect is less obvious at Ku-band. Unlike at C-band, Ku-band HH-polarized data better match the nearest IWRAP GMFs despite the large difference in incidence angle. Though this is not the expected geophysical behavior, the Ku-band HH-pol IWRAP GMF has a flatter response than does the VV-pol GMF. Both GMFs saturate at the same wind speed, but the VV-pol GMF is steeper than HH-pol both below and above the saturation speed. It is known that as the incidence angle draws closer to nadir, the slope of the A_0 response to wind speed becomes negative, which results in higher NRCS at lower wind speeds. Near 20° incidence, this ef-

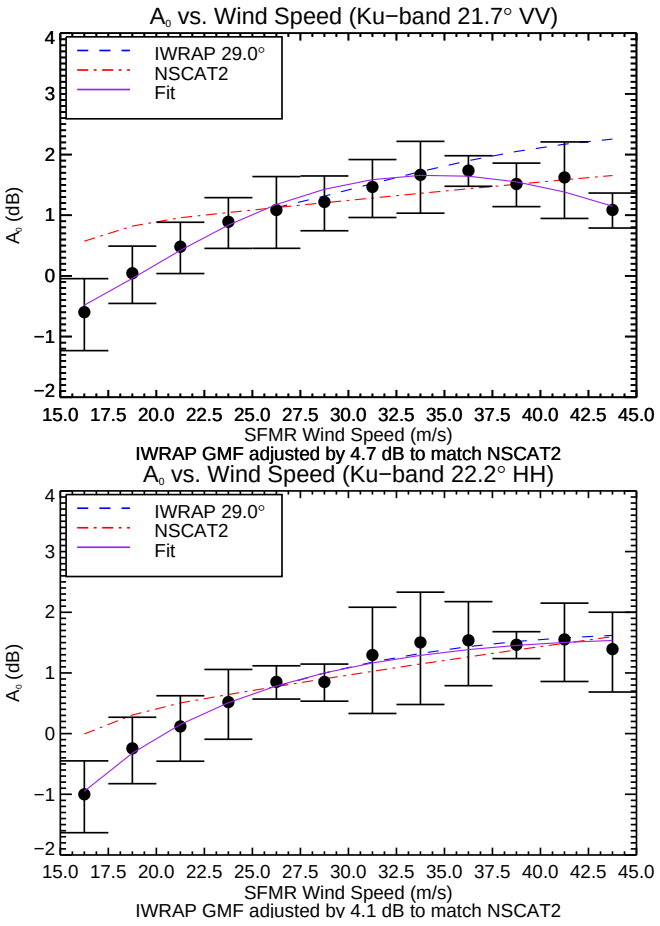

Fig. 3. Ku-band mean NRCS vs. wind speed (A_0 term) for 22° incidence, VV-polarization (top) and HH-polarization (bottom). A_0 data are shown as filled circles with the standard deviation of A_0 estimates from all wind vector cells shown as the error bars. GMFs shown where valid are IWRAP (dashed) and NSCAT2 (dash-dotted). The fit to the data is shown as a solid line.

fect may begin to manifest itself as a lower saturation wind speed and a low slope in A_0 with wind speed. As a result, for low incidence angle measurements at Ku-band the IWRAP HH-pol GMF will be closer to the data than the VV-pol GMF. This is primarily due to the relatively low slope of the IWRAP HH-pol A_0 GMF. More data is needed to verify the results at the highest wind speeds observed.

6. REFERENCES

[1] D. E. Fernandez, J. R. Carswell, S. Frasier, P. S. Chang, P. G. Black, and F. D. Marks, "Dual-polarized C- and Ku-band ocean backscatter response to hurricane-force winds," *Journal of Geophysical Research*, vol. 111, no. C8, 2006.

[2] D. E. Fernandez, E. M. Kerr, A. Castells, J. R. Carswell, S. J. Shaffer, P. S. Chang, P. G. Black, and F. D. Marks, "IWRAP: The Imaging Wind and Rain Airborne Profiler for remote sensing of the ocean and the atmospheric boundary layer within tropical cyclones," *IEEE Transactions on Geoscience and Remote Sensing*, vol. 43, no. 8, pp. 1775–1787, 2005.

[3] Bradley W. Klotz and Eric W. Uhlhorn, "Improved Stepped Frequency Microwave Radiometer Tropical Cyclone Surface Winds in Heavy Precipitation," *Journal of Atmospheric and Oceanic Technology*, vol. 31, no. 11, pp. 2392–2408, Nov. 2014.

[4] Eric W. Uhlhorn, Peter G. Black, James L. Franklin, Mark Goodberlet, James Carswell, and Alan S. Goldstein, "Hurricane Surface Wind Measurements from an Operational Stepped Frequency Microwave Radiometer," *Monthly Weather Review*, vol. 135, no. 9, pp. 3070–3085, 2007.

[5] H. Hersbach, A. Stoffelen, and S. de Haan, "An improved C-band scatterometer ocean geophysical model function: CMOD5," *Journal of Geophysical Research*, vol. 112, no. C3, Mar. 2007.

[6] P. W. Vachon and J. Wolfe, "C-Band Cross-Polarization Wind Speed Retrieval," *IEEE Geoscience and Remote Sensing Letters*, vol. 8, no. 3, pp. 456–459, 2011.

[7] Eric W. Uhlhorn and Peter G. Black, "Verification of Remotely Sensed Sea Surface Winds in Hurricanes," *Journal of Atmospheric and Oceanic Technology*, vol. 20, no. 1, pp. 99, Jan. 2003.